Dalton Transactions

Accepted Manuscript

ROYAL SOCIETY OF CHEMISTRY

www.rsc.org/dalton

Electrocatalytic proton reduction catalysed by the low-valent tetrairon-oxo cluster $[Fe_4(CO)_{10}(\kappa^2\text{-dppn})(\mu_4\text{-O})]^{2-}$ [dppn = 1,1′-bis(diphenylphosphino) naphthalene]

Shishir Ghosh,[a] Katherine B. Holt,[a] Shariff E. Kabir,[b] Michael G. Richmond[c] and Graeme Hogarth[a,d*]

[a] *Department of Chemistry, University College London, 20 Gordon Street, London WC1H OAJ, UK*

[b] *Department of Chemistry, Jahangirnagar University, Savar, Dhaka-1342, Bangladesh*

[c] *Department of Chemistry, University of North Texas, 1155 Union Circle, Box 305070, Denton, TX 76203, USA*

[d] *Department of Chemistry, King's College London, Britannia House, 7 Trinity Street, London SE1 1DB, UK. Email: graeme.hogarth@kcl.ac.uk*

Abstract: The 62-electron oxo-capped tetrairon butterfly cluster, $Fe_4(CO)_{10}(\kappa^2\text{-dppn})(\mu_4\text{-O})$ (**1**) {dppn = 1,8-bis(diphenylphosphino)naphthalene}, undergoes reversible one-electron oxidation and reduction events to generate the 61- and 63-electron radicals $[Fe_4(CO)_{10}(\kappa^2\text{-dppn})(\mu_4\text{-O})]^+$ ($\mathbf{1}^+$) and $[Fe_4(CO)_{10}(\kappa^2\text{-dppn})(\mu_4\text{-O})]^-$ ($\mathbf{1}^-$) respectively. Addition of a second electron affords the 64-electron cluster $[Fe_4(CO)_{10}(\kappa^2\text{-dppn})(\mu_4\text{-O})]^{2-}$ ($\mathbf{1}^{2-}$) which has more limited stability but is stable within the timeframe of the electrochemical experiment. While **1** and $\mathbf{1}^-$ are inactive as proton reduction catalysts, dianionic $\mathbf{1}^{2-}$ is active for the formation of hydrogen from both $CHCl_2CO_2H$ and CF_3CO_2H. This occurs *via* two separate mechanistic cycles branching at the mono-protonated species $[Fe_4(CO)_{10}(\kappa^2\text{-dppn})(\mu_4\text{-O})H]^-$ ($\mathbf{1H}^-$) resulting from the rapid protonation of $\mathbf{1}^{2-}$. This intermediate then undergoes competing protonation and reduction events leading to EECC and ECEC catalytic cycles respectively with $\mathbf{1}^-$ being pivotal to both. In order to understand the nature of $[Fe_4(CO)_{10}(\kappa^2\text{-dppn})(\mu_4\text{-O})]^{2-}$ ($\mathbf{1}^{2-}$) and its protonated products density functional theory (DFT) calculations have been employed. Theoretical calculations reveal that the cluster core remains intact in $\mathbf{1}^{2-}$, but the two consecutive one-electron reductions lead to an expansion of one of the trigonal-pyramids of this trigonal-bipyramidal cluster. The two-electron reduced cluster $\mathbf{1}^{2-}$ protonates at dppn-bound iron, accompanied by a wingtip-hinge iron-iron bond scission, and then reacts with a second proton to evolve hydrogen.

Introduction

The development of iron-based electrocatalysts capable of reducing protons to hydrogen is an area of intense research activity, this being predominantly focused on model complexes of the active site of the [FeFe]-hydrogenase enzyme [**1**]. In contrast to the multitude of contributions developing this theme, the ability of non-enzyme-related iron complexes to catalyse proton reduction has been neglected. Iron-containing low valent clusters are potentially useful in this respect as the highly delocalised nature of the bonding within the cluster core can give rise to low reduction potentials and stable reduced species [**2**]. Thus, metal carbonyl clusters have been shown to undergo a wide-range of reversible redox transformations and in some cases up to a significant number of stable redox states are accessible [**3**]. Berben and co-workers have recently reported that the tetrairon clusters $[NEt_4][Fe_4(CO)_{12}(\mu_4\text{-}N)]$ [**4,5**] and $[NEt_4]_2[Fe_4(CO)_{12}(\mu_4\text{-}C)]$ [**5**] are both efficient catalysts for the reduction of protons to hydrogen. Further, replacing the cation(s) with sodium leads to formation of water-soluble species which are able to generate hydrogen from aqueous acidic solutions [**5**]. Such clusters are potentially interesting catalysts as they are (in theory) able to bind hydrogen atoms to both electropositive metal centres (hydridic) and the (relatively) electronegative main group elements (acidic). Such binding is believed to be important in hydrogenases [**6**] and other catalytic processes [**7**] whereby acidic and hydridic hydrogens are held in close proximity (Chart).

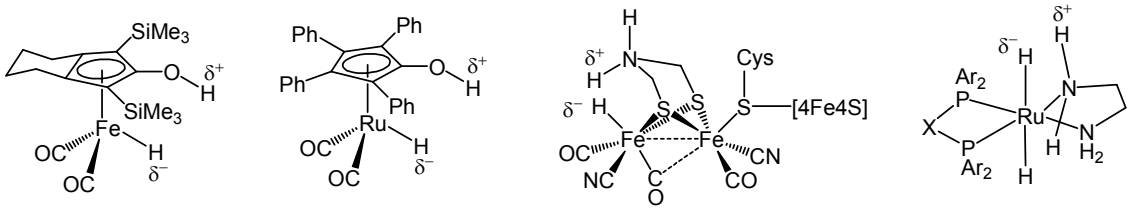

Chart Catalysts employing the co-coordination of acidic and hydridic hydrogen atoms

Low valent transition metal clusters containing oxo ligands are relatively rare as the latter is considered to be a *hard* π-donor ligand, while the cluster core is best stabilised by *soft* π-acceptor ligands [**8**]. For iron the most notable example of such an oxo cluster is $[Fe_3(CO)_9(\mu_3\text{-}O)]^{2-}$, formed in high yields from the reaction of oxygen with $[Fe_3(CO)_{11}]^{2-}$ [**9**]. In 2009 we reported the synthesis and crystal structure of the novel tetrairon-oxo cluster,

$Fe_4(CO)_{10}(\kappa^2$-dppn)(μ_4-O) (**1**) {dppn = 1,8-bis(diphenylphosphino)naphthalene}, formed in low yields from the reaction of dppn with $Fe_3(CO)_{12}$ [**10**]. This cluster is seemingly closely related to both of the isoelectronic clusters $[Fe_4(CO)_{12}(\mu_4\text{-N})]^-$ [**11**] and $[Fe_4(CO)_{12}(\mu_4\text{-C})]^{2-}$ [**12**], although DFT calculations suggested that it was best considered as a Lewis acid-base pair of $[Fe_3(CO)_9(\mu_3\text{-O})]^{2-}$ and $[Fe(CO)(\kappa^2\text{-dppn})]^{2+}$ [**10**], since the binding of the oxo ligand to the butterfly array of metal atoms was rather unsymmetrical. In contrast, both $[Fe_4(CO)_{12}(\mu_4\text{-N})]^-$ [**11**] and $[Fe_4(CO)_{12}(\mu_4\text{-C})]^{2-}$ [**12**] have approximate C_2-symmetry with the main-group atom binding equally to both wingtip metal atoms.

The oxo cluster $Fe_4(CO)_{10}(\kappa^2$-dppn)(μ_4-O) (**1**) thus seemed a potentially useful candidate for assessment as a proton reduction catalyst as reduction may lead to scission of the oxo-Lewis acid interaction leaving a three-coordinate oxo ligand and an iron(0) centre, the former generating a site for an acidic hydrogen and the latter for a hydridic hydrogen ion. Herein we provide details of the electrochemistry of **1** and show that, while in its neutral or singly reduced state it is not active for proton reduction, upon addition of two electrons the generated cluster dianion $[Fe_4(CO)_{10}(\kappa^2$-dppn)(μ_4-O)$]^{2-}$ ($\mathbf{1}^{2-}$) is an active proton reduction catalyst. Further we have used DFT calculations to probe the nature of $\mathbf{1}^{2-}$ and protonated derivatives leading to the development of a mechanistic overview of its operation *via* two different but inter-related catalytic cycles.

Results and discussion

Protonation studies

In our earlier work [**10**] we detailed preliminary studies on the protonation of $Fe_4(CO)_{10}(\kappa^2$-dppn)(μ_4-O) (**1**) using $HBF_4.Et_2O$ ($pK_a \approx 0.1$ in MeCN) [**13**] which resulted in the rapid (1-2 min) decolourization of the red solution with concomitant disappearance of all carbonyl bands. In order to try and develop conditions where **1** may be able to electrocatalyse the reduction of protons we screened its stability to a range of acids, monitoring this by IR spectroscopy. These results showed that it was stable in CH_2Cl_2 solution upon addition of excess Cl_2HCCO_2H ($pK_a \approx 13.2$ in MeCN) [**13**] and CF_3CO_2H ($pK_a \approx 12.7$ in MeCN) [**13**] as monitored by IR spectroscopy. Further the lack of any discernable changes to the IR spectrum in both cases (even after 2 h) indicated its inertness towards these acids in this

solvent (see ESI Figs. S1 and S2). Thus we conclude that **1** is stable in the presence of acids with pK_a values above 12.

Electrochemistry

The electrochemical response of **1** was studied by cyclic voltammetry (CV) in both CH_2Cl_2 and a 1:1 mixture of CH_2Cl_2/MeCN (since the electrocatalytic proton reduction by **1** was carried out in CH_2Cl_2/MeCN). Unfortunately we were unable to record good quality CVs in neat MeCN due to the poor solubility of **1** in this solvent. The CV of **1** recorded in CH_2Cl_2 at scan rate 0.1 V/s is shown in Fig. 1. In the cathodic region, it shows a reversible reduction at $E_{1/2}$ = –1.02 V, followed by a second irreversible reduction E_p = –1.59 V. The first reductive response remains unchanged at all scan rates, while the reversibility of the second reductive process improves at higher scan rates (≥0.5 V/s) (see ESI Fig. S3). The CV also shows a reversible oxidation in the anodic domain at $E_{1/2}$ = 0.74 V, which remains unchanged at all scan rates. All redox responses originate from the diffusion controlled solution process as shown by the linear i_p vs $\sqrt{v}$ plots (see ESI Fig. S4). We assume all the redox events observed in the CV of **1** involved one electron similar to those found in the related tetrairon nitride and carbide clusters [**4-5**]. These observations are consistent with formation of $[Fe_4(CO)_{10}(\kappa^2\text{-dppn})(\mu_4\text{-O})]^-$ (**1**$^-$) and $[Fe_4(CO)_{10}(\kappa^2\text{-dppn})(\mu_4\text{-O})]^+$ (**1**$^+$) which are stable within the timeframe of the experiment, and the dianion $[Fe_4(CO)_{10}(\kappa^2\text{-dppn})(\mu_4\text{-O})]^{2-}$ (**1**$^{2-}$) which has more limited stability, but nevertheless can be stable within the timeframe of the electrocatalytic transformations (see below).

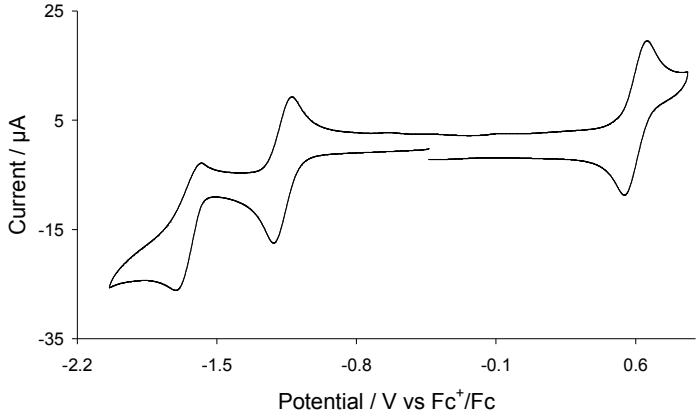

Fig. 1 CV of **1** in CH_2Cl_2 (1 mM solution, supporting electrolyte $[NBu_4][PF_6]$, scan rate 0.1 Vs^{-1}, glassy carbon electrode, potential vs Fc^+/Fc).

The CV of **1** in a 1:1 mixture of CH_2Cl_2/MeCN is shown in Fig. 2. The cathodic region shows similar reductive features to those observed in CH_2Cl_2, namely a reversible reduction at $E_{1/2}$ = –1.26 V followed by an irreversible process at E_p = –1.78 V. In contrast, the anodic region is quite different from that observed in CH_2Cl_2 and shows a large irreversible oxidative wave at E_p = 0.45 V, the peak height of which suggests more than one electron may be involved. Overall the redox responses in CH_2Cl_2/MeCN mixture appear at *ca.* 0.25 V more negative values than in CH_2Cl_2 alone. A new reduction peak is also seen at E_p = –1.46 V in CH_2Cl_2/MeCN when the anodic region is scanned first due to the reduction of product formed upon irreversible oxidation (see ESI Fig. S5). The height of this grows faster than the other reduction peaks as the scan rate is increased together with the appearance of an oxidative feature at E_p = –0.35 V on the return scan which is associated with this new reductive process (see ESI Figs. S6 and S7). The linear dependence of i_p against $\sqrt{v}$ shows all these redox events are diffusion controlled (see ESI Fig. S8).

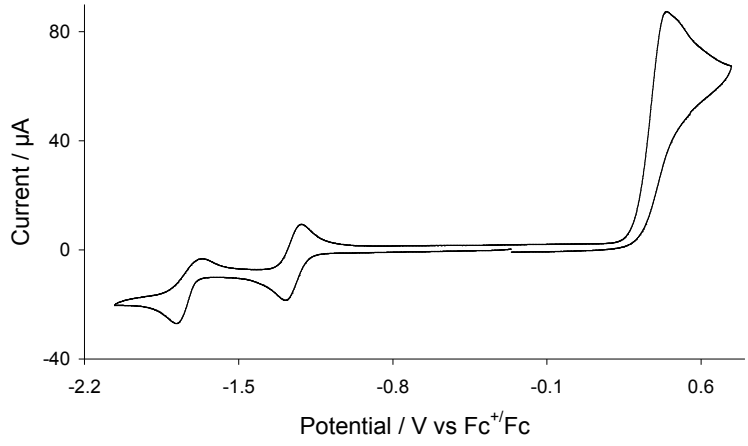

Fig. 2 CV of **1** in a 1:1 mixture of CH_2Cl_2/MeCN (1 mM solution, supporting electrolyte $[NBu_4][PF_6]$, scan rate 0.1 Vs^{-1}, glassy carbon electrode, potential vs Fc^+/Fc)

These observations are summarised in Scheme 1. Both the monoanion $\mathbf{1}^-$ and monocation $\mathbf{1}^+$ are stable in CH_2Cl_2 solutions, while in the presence of MeCN, $\mathbf{1}^+$ is clearly unstable and presumably degrades to species which are oxidised at lower potentials than **1** giving rise to the relatively large current observed. The dianion $\mathbf{1}^{2-}$ has some stability in CH_2Cl_2 and when MeCN is added this does not change significantly suggesting that MeCN does not coordinate to this cluster.

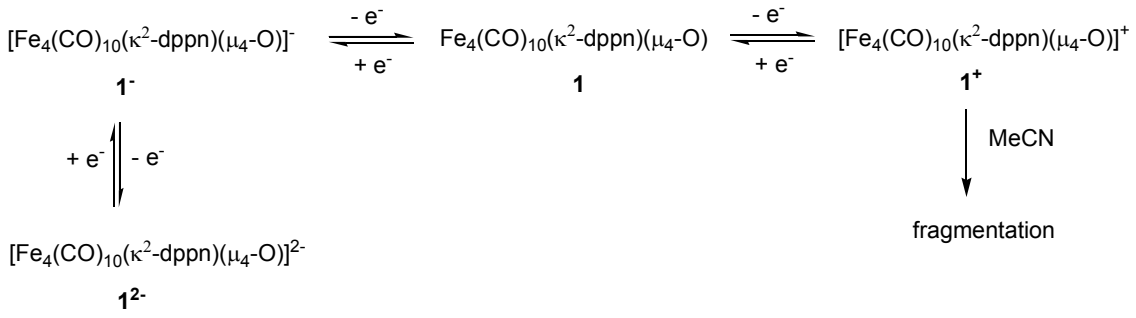

Scheme 1

The results of these studies compare well with those of Diego Rail and Berben on the isoelectronic nitride cluster $[NEt_4][Fe_4(CO)_{12}(\mu_4\text{-}N)]$ [**4**] when studied in MeCN. This shows a reversible one-electron reduction at –1.23 V vs SCE and a second irreversible reduction at –1.6 V *vs* SCE associated with generation of $[Fe_4(CO)_{12}(\mu_4\text{-}N)]^{2-}$ and $[Fe_4(CO)_{12}(\mu_4\text{-}N)]^{3-}$ respectively. Given the different solvents used in the two studies it is not easy to compare reduction potentials directly, although it is perhaps not surprising that the oxo cluster, with its lower charge and more electronegative main-group element, reduce at somewhat lower potentials than the nitride cluster. A perhaps more significant difference is the enhanced stability of $\mathbf{1}^{2-}$ over $[Fe_4(CO)_{12}(\mu_4\text{-}N)]^{3-}$ and this could be important regarding the proposed addition of two-electrons leading to Fe–O bond scission and the creation of vacant coordination sites on both atoms. One somewhat unexpected difference between the two clusters relates to their oxidation behaviour, with $\mathbf{1}^{+}$ showing significant stability in the absence of MeCN. Berben and co-workers recorded CVs of $[Fe_4(CO)_{12}(\mu_4\text{-}N)]^{-}$ in both MeCN [**4**] and water [**5**] and in both no stable oxidation product resulted. This may be simply a result of the strongly coordinating nature of both of these solvents.

Electrocatalysis

All electrocatalytic testing was carried out in a 1:1 mixture of CH_2Cl_2/MeCN. While the cation $\mathbf{1}^{+}$ is unstable in this medium, both the $\mathbf{1}^{-}$ and $\mathbf{1}^{2-}$ are stable on the electrochemical timeframe. Proton reduction catalysis was first tested with the relatively weak acid, CCl_2HCO_2H ($pK_a \approx 13.2$ in MeCN). Fig. 3 shows the CVs upon addition of up to 10 equivalents of acid to 1:1 mixture of CH_2Cl_2/MeCN solution of **1**. The second reduction peak shows *ca.* 70 mV positive shift with an increase in peak current upon addition of acid. The height of this peak grows slowly as the concentration of acid is increased, being characteristic of electrocatalytic proton reduction. A new catalytic peak is also seen at $E_p = –2.00$ V which

increases sharply with acid concentration, but the catalysis becomes competitive at this potential due to the direct reduction of CCl_2HCO_2H by the electrode.

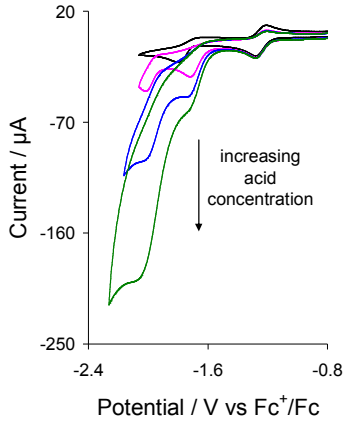

Fig. 3 CVs of **1** in the absence (black) and presence of 1 (pink), 4 (blue), 10 (green) equivalents of Cl_2HCCO_2H (in a 1:1 mixture of CH_2Cl_2/MeCN, 1 mM solution, supporting electrolyte $[NBu_4][PF_6]$, scan rate 0.1 Vs^{-1}, glassy carbon electrode, potential vs Fc^+/Fc).

In order to enhance the catalytic performance of **1** we carried out catalysis in presence of the stronger acid CF_3CO_2H. Fig. 4 shows the CVs upon addition of between 1-10 equivalents of CF_3CO_2H. Akin to the catalytic event(s) observed with Cl_2HCCO_2H, cluster **1** triggers a catalytic wave at its second reduction potential upon addition of CF_3CO_2H together with a second catalytic wave at E_p = –2.0 V but with well-resolved current. However, in this case the acid is not seen to reduce at the electrode within the potential range at which catalysis takes place and thus all catalytic current can be attributed to the reduction of protons by **1**. The catalytic current of the second wave is almost double than that of the first wave, and the current obtained with CF_3CO_2H is also much better higher than that with CCl_2HCO_2H, as might be expected for a stronger acid. The height of the oxidation peak remains unchanged upon addition of 10 equivalents CF_3CO_2H indicating no sign of degradation during catalysis.

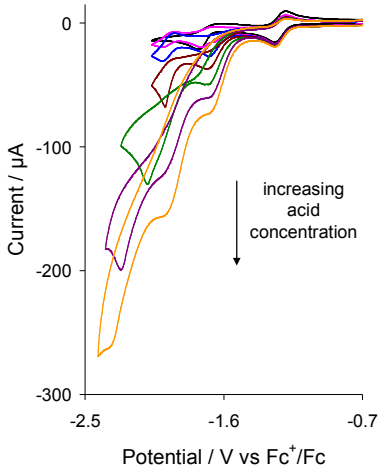

Fig. 4 CVs of **1** in the absence (black) and in the presence of 1 (pink), 2 (blue), 3 (brown), 5 (green), 8 (violate) and 10 (orange) equivalents of CF_3CO_2H (in a 1:1 mixture of CH_2Cl_2/MeCN, 1 mM solution, supporting electrolyte $[NBu_4][PF_6]$, scan rate 0.1 Vs^{-1}, glassy carbon electrode, potential vs Fc^+/Fc).

Density functional theory (DFT) calculations

In order to understand the structural consequences of electron addition to **1** and also in an attempt to identify likely protonation sites in order to support a clear mechanistic scheme for proton reduction, we have carried out a series of DFT calculations on **1**, $\mathbf{1}^-$ and $\mathbf{1}^{2-}$. Initially we sought to reproduce the ground state structure of **1** as elucidated by X-ray crystallography [**10**]. Calculations show that in the ground state the hinge Fe–Fe bonding orbital is the major component of the HOMO while the LUMO is delocalised over all five atoms constituting the trigonal-bipyramidal core of the cluster and the naphthalene ring (Fig. 5). After two-electron reduction, the HOMO of the reduced species ($\mathbf{1}^{2-}$) looks similar to the LUMO of neutral **1**, and the LUMO is now localized over the naphthalene ring and adjacent iron (Fig. 6).

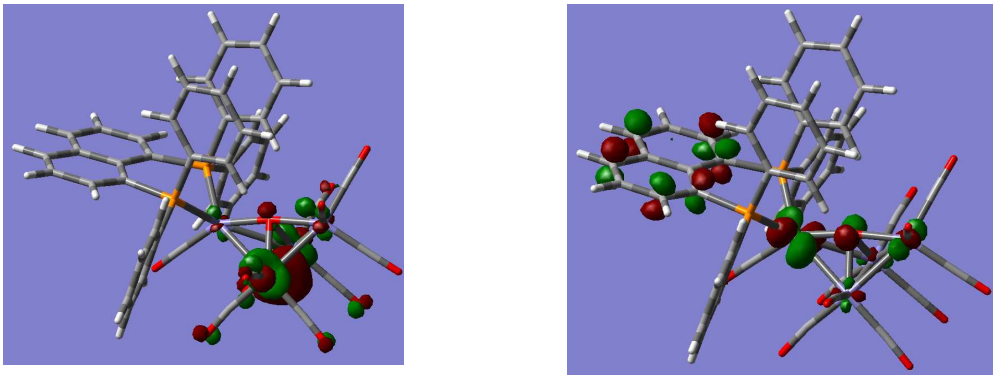

HOMO **LUMO**

Fig. 5 HOMO and LUMO of $Fe_4(CO)_{10}(\kappa^2\text{-dppn})(\mu_4\text{-O})$ (**1**).

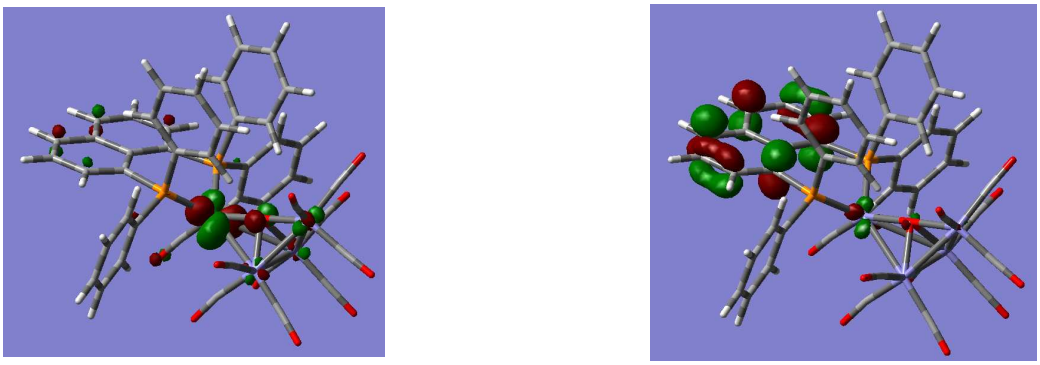

HOMO **LUMO**

Fig. 6 HOMO and LUMO of $[Fe_4(CO)_{10}(\kappa^2\text{-dppn})(\mu_4\text{-O})]^{2-}$ ($\mathbf{1}^{2-}$).

Analysis of atomic charges (Table 1) reveals that in $\mathbf{1}^{2-}$ the negative charge is mainly accumulated on the iron atom directly bonded to dppn ligand. The Wiberg bond index for Fe_1–Fe_2 and Fe_1–Fe_3 bonds are 0.28 and 0.29 respectively in **1** and 0.13 in $\mathbf{1}^{2-}$ (Table 1), the latter value is 46% smaller than those vectors in the neutral cluster, which suggests that these two bonds weaken considerably after two-electron reduction. The values for the Fe_1–O(oxo) bonds also decrease from 0.61 (in **1**) to 0.45 (in $\mathbf{1}^{2-}$) while the change in the indices for other three Fe–O(oxo) bonds are insignificant. Overall, two-electron reduction of **1** promotes the expansion of the trigonal-pyramid containing the dppn-substituted iron centre and does not lead to scission of any of the Fe–O(oxo) bonds.

Table 1. Selected natural charges and Wiberg bond indices for clusters **1** and $\mathbf{1}^{2-}$.[a]

Species	1	1^{2-}
Atomic Charge		
Fe_1	–0.62	–0.80
Fe_2	–1.26	–1.22
Fe_3	–1.26	–1.22
Fe_4	–1.10	–1.23
P_1	1.31	1.23
P_2	1.30	1.23
O(oxo)	–0.37	–0.44
Wiberg bond index		
Fe_1–Fe_2	0.28	0.13
Fe_1–Fe_3	0.29	0.13
Fe_2–Fe_3	0.52	0.49
Fe_2–Fe_4	0.44	0.45
Fe_3–Fe_4	0.44	0.45
Fe_1–P_1	0.73	0.68
Fe_3–P_2	0.73	0.68
Fe_1–O(oxo)	0.61	0.45
Fe_2–O(oxo)	0.51	0.54
Fe_3–O(oxo)	0.52	0.55
Fe_4–O(oxo)	0.59	0.55

[a]Atom numbers for species **1** and $\mathbf{1}^{2-}$ are based on the numbering sequence for the structure depicted below:

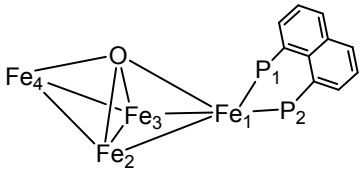

Mechanistic considerations

Berben and co-workers have addressed the mechanism of proton reduction with $[Fe_4(CO)_{12}(\mu_4\text{-}N)]^-$ as a pre-catalyst both in MeCN [**4**] and in aqueous solutions [**5**]. The major features of the catalysis do not vary significantly with changes in solvent and an ECCE mechanism is favoured (Scheme 2). Thus, $[Fe_4(CO)_{12}(\mu_4\text{-}N)]^-$ is not catalytically active and nor does it bind protons strongly. Thus in MeCN, catalysis occurs at the potential of the one-electron reduced species, $[Fe_4(CO)_{12}(\mu_4\text{-}N)]^{2-}$, showing that this is a key catalytic intermediate. This cluster protonates readily to afford $[Fe_4(CO)_{12}(\mu_4\text{-}N)H]^-$ and it is protonation of this species to give $[Fe_4(CO)_{12}(\mu_4\text{-}N)H_2]$ which is rate-limiting, with subsequent reduction and loss of hydrogen being facile. This is in accord with their experimental observation that the strength of the acid is a key factor in the rate of the hydrogen evolution reaction [**4**]. In water, a similar reaction scheme is proposed [**5**] and here $[Fe_4(CO)_{12}(\mu_4\text{-}N)H]^-$ was directly observed *via* its oxidation to yield $[Fe_4(CO)_{12}(\mu_4\text{-}N)H]$. Berben and co-workers did not attempt to identify proton binding sites or delineate structural changes to the cluster upon reduction.

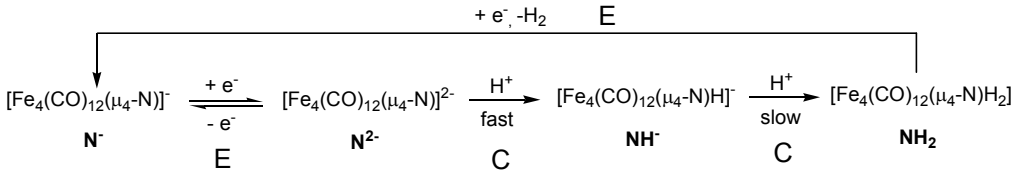

Scheme 2

In contrast, when $[Fe_4(CO)_{12}(\mu_4\text{-}C)]^{2-}$ was employed as a pre-catalyst in water a significantly different mechanistic scheme for proton reduction was seen (Scheme 3). Now protonation of the dianion was coupled with reduction to afford $[Fe_4(CO)_{12}(\mu_4\text{-}C)H]^{2-}$ which in turn undergoes a second proton-coupled electron transfer to afford $[Fe_4(CO)_{12}(\mu_4\text{-}C)H_2]^{2-}$ with liberation of hydrogen closing the catalytic cycle [**5**].

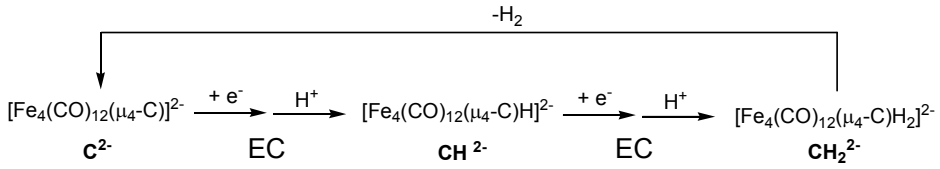

Scheme 3

On the basis of the electrochemical and electrocatalytic results when **1** is used as a pre-catalyst we propose that two interlinked catalytic cycles are operating, the relative rates of which are dependent upon acid type and concentration (Scheme 4).

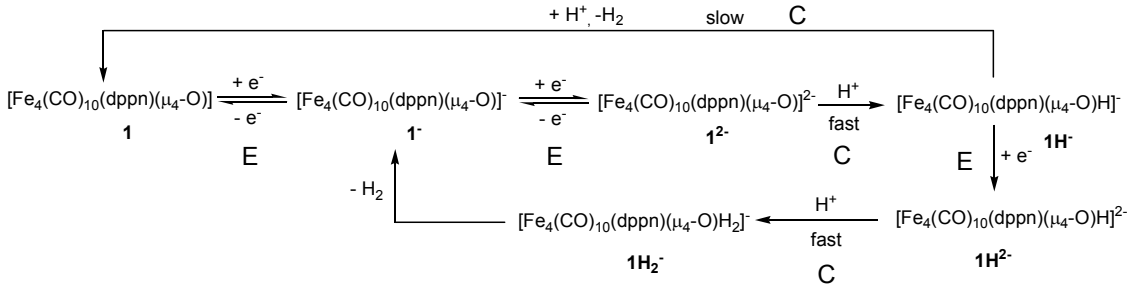

Scheme 4

Thus, it is clear from both Figs. 3 and 4 that $[Fe_4(CO)_{10}(\kappa^2\text{-dppn})(\mu_4\text{-O})]^-$ (**1**$^-$) is not catalytically active and that two catalytic process operate on at the approximate reduction potential of **1**$^-$ which clearly involves formation of $[Fe_4(CO)_{10}(\kappa^2\text{-dppn})(\mu_4\text{-O})]^{2-}$ (**1**$^{2-}$) and the second which takes place at around –2.0 V, a potential that is not associated with any unprotonated tetrairon-oxo species. In order to account for these observations we suggest that protonation of **1**$^{2-}$ is rapid and generates $[Fe_4(CO)_{10}(\kappa^2\text{-dppn})(\mu_4\text{-O})H]^-$ (**1H**$^-$) which can then either undergo a second protonation to afford $Fe_4(CO)_{10}(\kappa^2\text{-dppn})(\mu_4\text{-O})H_2$ (**1H$_2$**) (not shown) and either this event or loss of hydrogen is rate-limiting to regenerate **1** *via* an overall EECC mechanism. Given the slow rate of protonation of **1H**$^-$ it has a life-time long enough to undergo a further reduction to generate **1H**$^{2-}$ a process which occurs at *ca.* 2 V. Protonation of **1H**$^{2-}$ is then expected to be relatively rapid with loss of hydrogen resulting in generation of **1**$^-$. Thus, this overall process proceeds *via* an ECEC mechanism. That the rate of protonation of **1H**$^-$ is the determining factor regarding the relative amounts of hydrogen generated by each cycle is supported by experiments using different acids. Thus with the relatively weak acid Cl_2HCCO_2H (pK_a = 13.2) the current from the lower potential process does not vary significantly upon addition of excess acid, while that associated with the second process does.

In contrast, with CF_3CO_2H (pK_a = 12.7) both processes increase notably upon successive addition of acid although the rate of increase of the ECEC process (at –2.0 V) is faster than that for the EECC cycle.

Since two-electron reduction leads to expansion of one of the trigonal-pyramids of **1** instead of Fe–O or Fe–Fe bond scission, it is difficult to identify the proton binding site in $\mathbf{1}^{2-}$. To identify this and also to understand the structural changes taking place during catalysis, we probed the EECC catalytic cycle by DFT calculations. These show that protonation takes place at the dppn-bound iron in $\mathbf{1}^{2-}$, with concomitant cleavage of one of the wingtip-hinge Fe–Fe bonds (Fig. 7a), to form $\mathbf{1H}^-$. The negative charge is mainly accumulated on the dppn-bound iron atom in $\mathbf{1}^{2-}$, as shown by the atomic charge analysis which also supports this protonation behaviour (Table 1). The second wingtip-hinge Fe–Fe bond involving this iron is also found to be significantly longer after protonation with a bond distance of 2.761 Å as compared to the average wingtip-hinge Fe–Fe bond distance of 2.650 Å in **1**. However, the Wiberg bond index suggests a weak bonding interaction between these two iron atoms. The second protonation lead to the formation of a hydrogen complex, $\mathbf{1H_2}$, in which hydrogen is bonded to the dppn-bound iron atom (Fig. 7b). This species releases hydrogen and regenerates **1** *via* the 62-electron cluster **1′** which has an open Fe–Fe edge as shown in Scheme 5. Cluster **1′** can either undergo two-electron reduction to regenerate the dianion $\mathbf{1}^{2-}$ or undergo bond closure to regenerate the starting cluster **1**, and the energy difference between **1** and **1′** is only *ca.* 2 kcalmol^{-1} in the gas phase (Fig. 8).

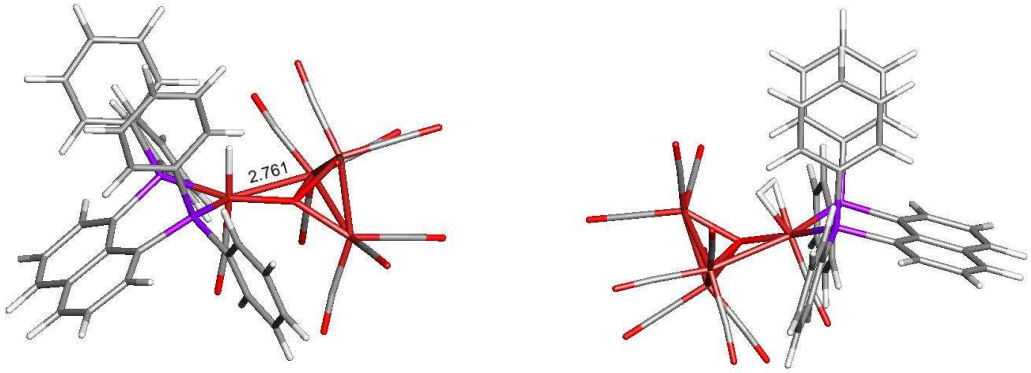

(a) (b)

Fig. 7 B3LYP-optimized structure of $[Fe_4(CO)_{10}(\kappa^2\text{-dppn})(\mu_4\text{-O})H]^-$ ($\mathbf{1H}^-$) and $Fe_4(CO)_{10}(\kappa^2\text{-dppn})(\mu_4\text{-O})H_2$ ($\mathbf{1H_2}$).

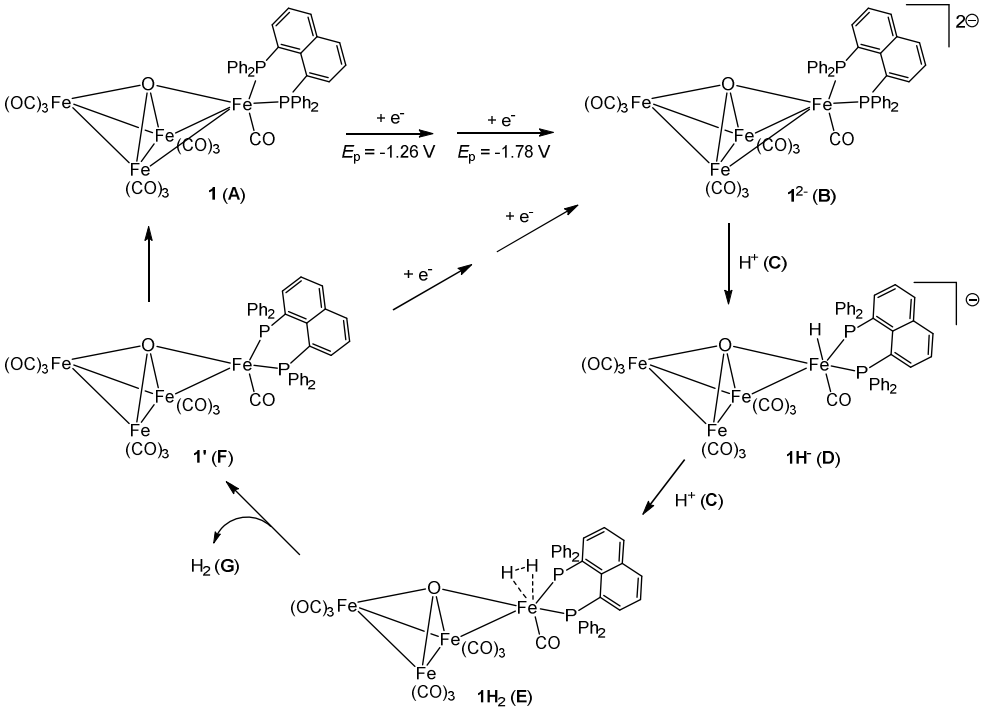

Scheme 5. Proposed mechanism for electrocatalytic proton reduction by **1**

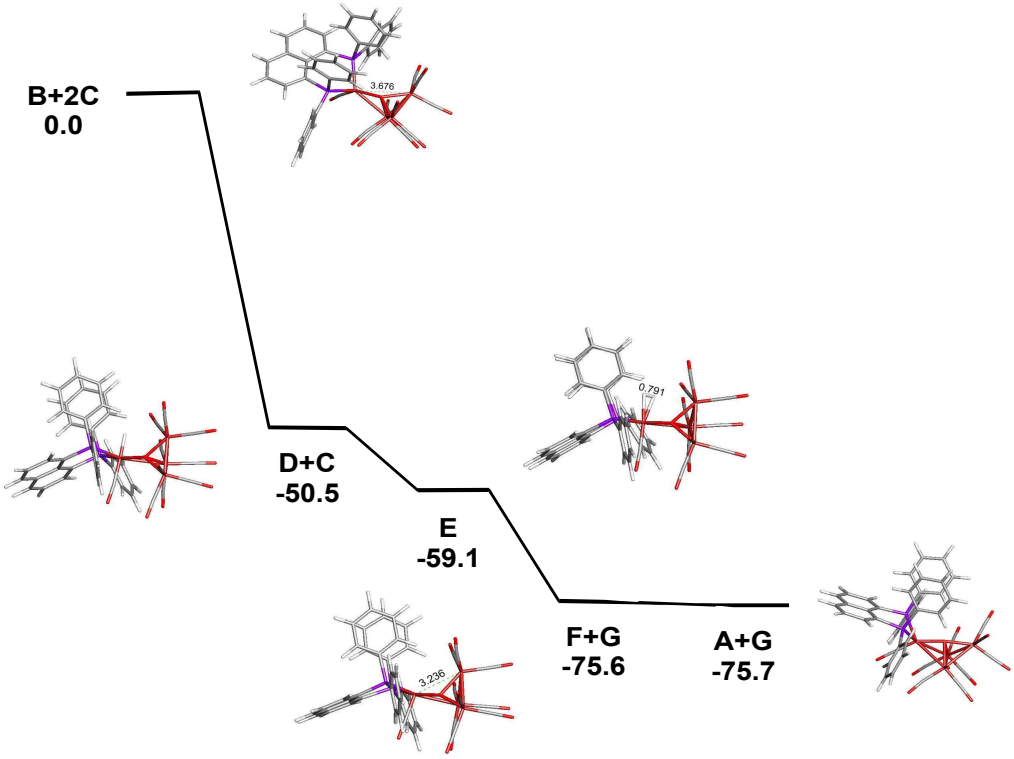

Fig. 8 B3LYP-optimized structures and free energy surface for the reaction of the dianion $\mathbf{1}^{2-}$ (**B**) with H^+ (**C**). Energy values are in kcalmol^{-1} with respect to **B**+**2C**. The optimized structure of the liberated H_2 (**G**) that accompanies **1′** (**F**) and **1** (**A**) is not shown.

Conclusions

The tetrairon-oxo cluster $Fe_4(CO)_{10}(\kappa^2\text{-dppn})(\mu_4\text{-O})$ (**1**) has been studied as a proton reduction catalyst. The cluster contains a trigonal bipyramidal core consists of an oxygen and four iron atoms. Acidification studies show that **1** is stable in presence of acid with pK_a >12 but does not undergo protonation. It degrades rapidly in presence of strong acid such as $HBF_4{\cdot}Et_2O$ (pK_a ≈ 0.1 in MeCN). The cluster undergoes two sequential one-electron reductions to generate $\mathbf{1}^-$ and $\mathbf{1}^{2-}$ respectively which are stable on the voltammetric timescale. The oxidised species $\mathbf{1}^+$ is also stable in CH_2Cl_2 but undergoes fragmentation (probably by reacting with MeCN) when 1:1 mixture of CH_2Cl_2/MeCN was used as solvent. Electrocatalytic studies carried out in presence of Cl_2HCCO_2H and CF_3CO_2H show that **1** becomes catalytically active at its second reduction potential with the catalytic current depending on acid strength. At least two competitive catalytic cycles are involved in the proton reduction event by **1** leading to two distinct catalytic waves in presence of acid.

DFT calculations carried out to identify the proton binding site and structural changes during catalysis show that the cluster remains intact after two-electron reduction. One of the trigonal pyramids expand by this process instead of Fe–Fe or Fe–O(oxo) bond cleavage, the latter being highly expected since **1** was best described as a Lewis acid-base pair of $[Fe_3(CO)_9(\mu_3\text{-O})]^{2-}$ and $[Fe(CO)(\kappa^2\text{-dppn})]^{2+}$ [**10**]. Cluster $\mathbf{1}^{2-}$ protonates at the wingtip iron bonded to dppn with concomitant rupture of one of the wingtip-hinge Fe–Fe bonds. Overall results suggest that the $[Fe_3(CO)_9(\mu_3\text{-O})]^{2-}$ moiety acts as a bidentate ligand to $[Fe(CO)(\kappa^2\text{-dppn})]^{2+}$ fragment where the catalysis takes place and the oxygen atom has no direct role in the catalysis, although its electronegativity probably serves to stabilise generated anionic species.

Experimental section

General Procedures and Starting Materials

Cluster **1** was prepared according to the literature method [**10**]. IR spectra were recorded using a Nicolet 6700 FT-IR spectrometer in a solution cell fitted with calcium fluoride plates, subtraction of the solvent absorptions being achieved by computation.

Electrochemical Studies

Electrochemistry was carried out either in deoxygenated CH_2Cl_2 or a 1:1 mixture of CH_2Cl_2/MeCN with 0.1 M $TBAPF_6$ as the supporting electrolyte. The working electrode was a 3 mm diameter glassy carbon electrode that was polished with 0.3 μm alumina slurry prior to each scan. The counter electrode was a Pt wire and the quasi-reference electrode was a silver wire. All CVs were referenced to the Fc^+/Fc redox couple. An Autolab potentiostat (EcoChemie, Netherlands) was used for all electrochemical measurements. Catalysis studies were carried out by adding equivalents of Cl_2HCCO_2H or CF_3CO_2H (Sigma-Aldrich).

Computational Methodology

DFT calculations were performed with the Gassian09 package of programs [**14**]. The calculations were carried out with the B3LYP functional, which utilizes the Becke three-parameter exchange functional (B3) [**15**] combined with the correlation functional of Lee, Yang, and Parr (LYP) [**16**]. The iron atoms were described by Stuttgart-Dresden effective core potentials (ecp) and an SDD basis set, while the 6-31+G(d') basis set was employed for the remaining atoms.

The geometries reported for all species were fully optimized and the analytical Hessian afforded only positive eigenvalues for each ground-state structure. The computed frequencies were used to make zero-point and thermal corrections to the electronic energies, and the reported free energies are quoted in kcal/mol relative to the specified standard. The computed frequencies were used to make zero-point and thermal corrections to the electronic energies.

In order to evaluate the thermodynamics for proton reduction, the solvation energy of proton [$\Delta G_{solv}(H^+)$] was determined in dichloroethane (DCE) using the known pK_a of phenol (19.6) and the following equation:

$$\Delta G_{solv}(H^+) = \Delta G_{solv}(HA) - \Delta G_{solv}(A^-) + 2.303RTpK_a$$

The effect of DCE solvent on all iron-containing species was calculated using the polarizable continuum model (PCM) through single-point calculations of the gas-phase optimized geometry. The resulting solvation free energy was appropriately added to the

ΔG_{gas} to yield ΔG_{solv}. Use of DCE in place of DCM as the solvent was dictated by the availability of the pK_a data for a wide variety of acid-base equilibria in the former solvent [**17**]. Standard-state corrections were added to all species to convert concentrations from 1 atm to 1 M, as outlined in the treatise by Cramer [**18**].

The Wiberg bond indices were computed using Weinhold's natural bond orbital (NBO) program, as executed by Gaussian 09 [**19**,**20**]. The geometry-optimized structures were drawn with the *JIMP*2 molecular visualization and manipulation program [**21**,**22**].

Acknowledgements

We thank the Commonwealth Scholarship Commission for the award of a Commonwealth Scholarship to SG. MGR acknowledges financial support from the Robert A. Welch Foundation (Grant B-1093) and the NSF (CHE-0741936). Prof. Michael B. Hall (TAMU) is thanked for providing us a copy of his JIMP2 program, which was used to prepare the geometry optimized structures reported here.

References

[1] (a) I.P. Georgakaki, L.M. Thomson, E.J. Lyon, M.B. Hall, M.Y. Darensbourg, *Coord. Chem. Rev.*, 2003, **238-239**, 255; (b) D.J. Evans, C.J. Pickett, *Chem. Soc. Rev.,* 2003, **32**, 268; (c) T.B. Rauchfuss, *Inorg. Chem.,* 2004, **43**, 14; (d) L. Sun, B. Åkermark, S. Ott, *Coord. Chem. Rev.,* 2005, **249**, 1653; (e) X. Liu, S.K. Ibrahim, C. Tard, C.J. Pickett, *Coord. Chem. Rev.,* 2005, **249**, 1641; (f) N. Wang, M. Wang, L. Chen, L. Sun, *Dalton Trans.,* 2013, **42**, 12059.

[2] (a) S. Ghosh, G. Hogarth, K.B. Holt, S.E. Kabir, A. Rahaman, D.G. Unwin, *Chem. Commun.,* 2011, **47**, 11222; (b) A. Rahaman, S. Ghosh, D.G. Unwin, S. Basak-Modi, K.B. Holt, S.E. Kabir, E. Nordlander, M.G. Richmond, G. Hogarth, *Organometallics,* 2014, **33**, 1356; (c) Z. Li, X. Zeng, Z. Niu, X. Liu, *Electrochimica Acta,* 2009, **54**, 3638; (d) J. Yeo, M. H. Cheah, M. I. Bondin, S. P. Best, *Aust. J. Chem.,* 2012, **65**, 241; (e) W. Gao, J. Sun, M. Li, T. Åkermark, K. Romare, L. Sun, B. Åkermark, *Eur. J. Inorg. Chem.,* 2011, 1100; (f) C.A. Mebi, K.E. Brigance, R.B. Bowman, *J. Braz. Chem. Soc.,* 2012, **23**, 186; (f) M.H. Cheah, C. Tard, S.J. Borg, X. Liu, S.K. Ibrahim,

C.J. Pickett, S.P. Best, *J. Am. Chem. Soc.*, 2007, **129**, 11085; (g) C. Tard, X. Liu, D.L. Hughes, C.J. Pickett, *Chem. Commun*., 2005, 133.

[3] (a) S.R. Drake, *Polyhedron*, 1990, **9**, 455; (b) G. Longoni, C. Femoni, M.C. Iapalucci, P. Zanello in Metal Clusters in Chemistry Eds. P. Braunstein, L.A. Oro, P.R. Raithby, 199, **2**, 1137; (c) G. Hogarth, S.E. Kabir, E. Nordlander, *Dalton Trans.,* 2010, **39**, 6153-6174; (d) T.M. Bockman, J.K. Kochi, *J. Am. Chem. Soc.,* 1987, **109**, 7725. (e) Q. Zhao, T.D. Harris, T.A. Betley, *J. Am. Chem. Soc.,* 2011, **133**, 8293; (f) R.J.H. Clark, P.J. Dyson, D.G. Humphrey, B.F.G. Johnson, *Polyhedron*, 1998, **17**, 2985; (g) M.P. Cifuentes, M.G. Humphrey, G.A. Heath, *Inorg. Chim. Acta,* 1997, **259**, 273.

[4] M.D. Rail, L.A. Berben, *J. Am. Chem. Soc.,* 2011, **133**, 18577.

[5] A.D. Nguyen, M.D. Rail, M. Shanmugam, J.C. Fettinger, L.A. Berben, *Inorg. Chem.* 2013, **52**, 12847.

[6] (a) H.J. Fan, M.B. Hall, *J. Am. Chem. Soc.,* 2001, **123**, 3828; (b) M. Bourrez, R. Steinmetz, F. Gloaguen, *Inorg. Chem.,* 2014, **53**, 10667; (c) J.-F. Capon, S. Ezzaher, F. Gloaguen, F.Y. Pétillon, P. Schollhammer, J. Talarmin, *Chem.-Eur. J.,* 2008, **14**, 1954.

[7] (a) C.P.Casey, H. Guan, *J. Am. Chem. Soc.,* 2007, **129**, 5816; (b) R. Noyori, T. Ohkuma, *Angew. Chem., Int. Ed.,* 2001, **40**, 40; (c) T. Ikariya, K. Murata, R. Noyori, *Org. Biomol. Chem.,* 2006, **4**, 393; (d) Y. Shvo, D. Czarkie, Y. Rahamim, D.F. Chodosh, *J. Am. Chem. Soc.,* 1986, **108**, 7400; (e) C.P. Casey, S.W. Singer, D.R. Powell, R.K. Hayashi, M. Kavana, *J. Am. Chem. Soc.,* 2001, **123**, 1090.

[8] (a) J.Y. Park, J.R. Shapley, C. Bueno, J.W. Ziller, M.R. Churchill, *Organometallics,* 1988, **7**, 2307; (b) L. Xu, K.H. Whitmire, *Organometallics,* 2002, **21**, 2581; (c) J.-H. Gong, D.-K. Hwang, C.-W. Tsay, Y. Chi, S.-M. Peng, G.-H. Lee, *Organometallics,* 1994, **13**, 1720; (d) M.R. Churchill, C. Bueno, J.T. Park, J.R. Shapley, *Inorg. Chem.,* 1984, **23**, 1017; (e) Y. Chi, L. Hwang, G.-H. Lee, S.-M. Peng, *J. Chem. Soc., Chem. Commun.,* 1988, 1456; (f) Y. Chi, J.R. Shapley, J. Ziller, M.R. Churchill, *Organometallics.* 1987, **6**, 301; (g) R.J. Goudsmit, B.F.G. Johnson, J. Lewis, P.R. Raithby, K.H. Whitmire, *J. Chem. Soc.*, *Chem. Commun.,* 1983, 246; (h) G. Lavigne, N. Lugan, J.-J. Bonnet, *Nouv. J. Chim.,* 1981, **5**, 423 ; (i) Md. D.H. Sikder, S. Ghosh, S.E. Kabir, G. Hogarth, D.A. Tocher, *Inorg. Chim. Acta,* 2011, **376**, 170; (j) C.K. Schauer, D.F. Shriver, *Angew. Chem., Int. Ed.,* 1987, **26**, 255; (k) C.K. Schauer, S. Harris, M. Sabat, E.J. Voss, D.F. Shriver, *Inorg. Chem.,* 1995, **34**, 5017.

[9] (a) A. Ceriotti, L. Resconi, F. Demartin, G. Longoni, M. Manassero, M. Sansoni, *J. Organomet. Chem.,* 1983, **249**, C35; (b) C. Femoni, M.C. Iapalucci, G. Longoni, S.

Zacchini, E. Zazzaroni, *Dalton Trans.,* 2007, 2644; (c) V.G. Albano, C. Castellari, C. Femoni, M.C. Iapalucci, G. Longoni, M. Monari, M. Rauccio, S. Zacchini, *Inorg. Chim. Acta,* 1999, **291**, 372; (d) L.A. Poliakova, S.P. Gubin, O.A. Belyakova, Y.V. Zubavichus, Y.L. Slovokhotov, *Organometallics,* 1997, **16**, 4527.

[10] S. Ghosh, G. Hogarth, S.E. Kabir, A.L. Miah, L. Salassa, S. Sultana, C. Garino, *Organometallics,* 2009, **28**, 7047.

[11] (a) D.E. Fjare, W.L. Gladfelter, *Inorg. Chem.,* 1981, **20**, 3533; (b) D.E. Fjare, W.L. Gladfelter, *J. Am. Chem. Soc.,* 1981, **103**, 1572; (c) P. Zanello, F. Laschi, A. Cinquantini, R.D. Pergola, L. Garlaschelli, M. Cucco, F. Demartin, T.R. Spalding, *Inorg. Chim. Acta,* 1994, **226**, 1; (d) M. Tachikawa, J. Stein, E.L. Muetterties, R.G. Teller, M.A. Beno, E. Gebert, J.M. Williams, *J. Am. Chem. Soc.,* 1980, **102**, 6648.

[12] (a) J.H. Davies, M.A. Beno, J.M. Williams, J. Zimmie, M. Tachikawa, E.L. Muetterties, *Proc. Natl. Acad. Sci. U.S.A.,* 1981, **78**, 668; (b) J.S. Bradley, G.B. Ansell, M.E. Leonowicz, E.W. Hill, *J. Am. Chem. Soc.,* 1981, **103**, 4968; (c) S. Harris, M.L. Blohm, W.L. Gladfelter, *Inorg. Chem.,* 1989, **28**, 2290; (d) M. Tachikawa, E.L. Muetterties, *J. Am. Chem. Soc.,* 1980, **102**, 4541; (e) M.A. Beno, J.M. Williams, M. Tachikawa, E.L. Muetterties, *J. Am. Chem. Soc.,* 1980, **102**, 4542.

[13] K. Izutsu, *in Acid-Base Dissociation Constants in Dipolar Aprotic Solvents*, Blackwell Scientific Publications, Oxford, 1990.

[14] M. J. Frisch *et al*., Gaussian 09, Revision E.01, Gaussian, Inc., Wallingford, CT, USA, 2009.

[15] A. D. Becke, *J. Chem. Phys.*, 1993, **98**, 5648.

[16] C. Lee, W. Yang and R. G. Parr, *Phys. Rev. B*, 1988, **37**, 785.

[17] E. Raamat, K. Kaupmees, G. Ovsjannikov, A. Trummal, A. Kütt, J. Saame, I. Koppel, I. Kaljurand, L. Lipping, T. Rodima, V. Pihl, I. A. Koppel, I. Leito, *J. Phys. Org. Chem.*, 2013, **26**, 162.

[18] C. J. Cramer, *Essentials of Computational Chemistry*, 2nd Ed.; Wiley: Chichester, UK, 2004, p. 378.

[19] A. E. Reed, L. A. Curtiss, F. Weinhold, *Chem. Rev.*, 1988, **88**, 899.

[20] K. B. Wiberg, *Tetrahedron*, 1968, **24**, 1083.

[21] JIMP2, version 0.091, a free program for the visualization and manipulation of molecules: M. B. Hall, R. F. Fenske, *Inorg. Chem.*, 1972, **11**, 768.

[22] J. Manson, C. E. Webster, M. B. Hall, Texas A&M University, College Station, TX, 2006: http://www.chem.tamu.edu/jimp2/index.html.

Table of contents

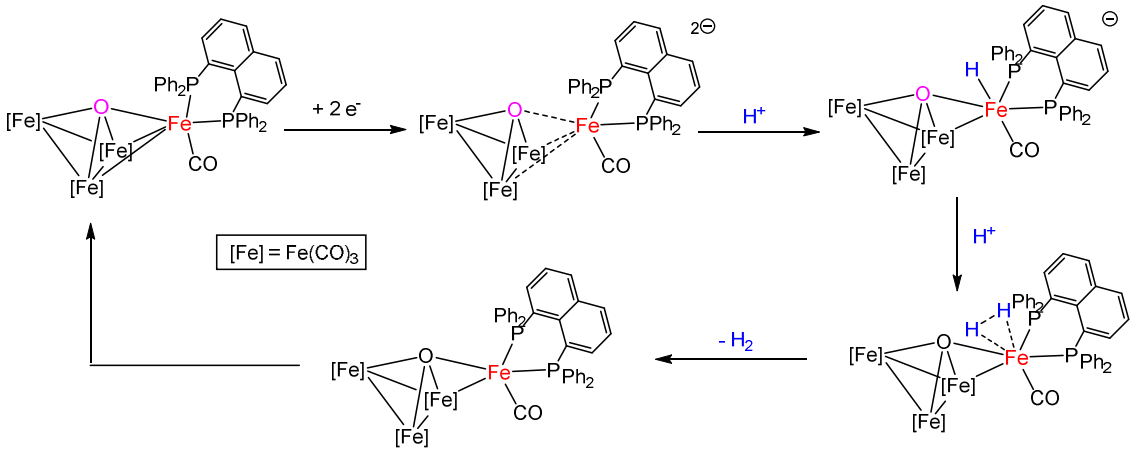

$[Fe_4(CO)_{10}(\kappa^2\text{-dppn})(\mu_4\text{-O})]^{2-}$ reduces protons and DFT calculations support the sequential formation of hydride and dihydrogen ligands at the unique iron centre.